

Physics-based Probabilistic Demand Model and Reliability Analysis for Reinforced Concrete Beams under Blast Loads

Flavio Stochino^{a,*}, Armin Tabandeh^b, Paolo Gardoni^b, Mauro Sassu^a

^a*Department of Civil Engineering, Environmental and Architecture, University of Cagliari, Building A - Via Marengo 2, 09123 Cagliari (CA), Italy*

^b*Department of Civil and Environmental Engineering, University of Illinois at Urbana-Champaign, 205 N. Mathews Ave., Urbana, IL 61801*

Abstract

This paper proposes a general physics-based probabilistic demand model for the reliability analysis of reinforced concrete (RC) beams under blast loading. The formulation of the proposed demand model builds on a computationally convenient representation of the governing physical laws from structural dynamics and adds a correction term and a model error. Specifically, the proposed demand model starts with predictions from a generalized single-degree-of-freedom (SDOF) representation of the RC beam, derived from the conservation law of energy; the correction term removes the implicit bias and improves the accuracy of the model, and the model error captures the remaining uncertainty in model predictions. Unknown model parameters are included in the correction term and the model error. Once formulated, the probabilistic model is calibrated with data from experimental tests or high-fidelity computational models. The inclusion of the governing physical laws in the proposed model avoids a strong dependence of the model on the specific data used for the model calibration. The paper uses Bayesian inference that combines predictions from the generalized SDOF representation with experimental data and any prior information to estimate the unknown model parameters. The paper then uses the proposed demand model in a formulation to estimate the reliability of RC beams under blast loading. Finally, the paper illustrates the novel contributions by estimating the reliability of an RC beam under blast loading for three damage levels. As part of the reliability analyses, the paper also identifies the dominant sources of uncertainty in estimating the failure probability.

Keywords: Probabilistic model, Reliability analysis, Bayesian inference, Differential equation, Blast loading.

*Corresponding author

Email addresses: fstochino@unica.it (Flavio Stochino), tabande2@illinois.edu (Armin Tabandeh), gardoni@illinois.edu (Paolo Gardoni), msassu@unica.it (Mauro Sassu)

1. Introduction

During their service lives, structures and infrastructure might be subject to blast loading from malicious or accidental explosions. The consequences of such extreme events can be catastrophic, ranging from economic losses to fatalities and social disruptions (e.g., Ronan Point (London) 1968 [1], New York 2001 [2], London 2005 [3], Beirut 2020 [4].) The performance of structures and infrastructure subject to explosive blast loading represents a complex nonlinear behavior due to the high amount of energy imparted to these systems over a short time. Governing differential equations can rigorously represent the complex nonlinear dynamics of structures and infrastructure under explosive blast loading. However, idealized mathematical representations of physical laws in differential equations, numerical errors in solution algorithms, and uncertainties in input data (e.g., blast load and materials mechanical characteristics) lead to discrepancies between predictions and the system's actual performance. Performance predictions require characterizing and propagating these uncertainties through the governing differential equations and quantifying their impact on systems responses. However, incorporating uncertainties in complex physical processes, like the behavior structures and infrastructure under explosive blast loading, represents a significant computational challenge.

Experimental tests [5–9] on reinforced concrete (RC) structures under blast loads have been the subject of much research and provided insights for developing mathematical models. For example, Zhang et al. [5] studied the scaling problem of RC beams under close-in blast loads with an experimental approach. Yao et al. [6] analyzed the damages of RC beams under field blast, while Magnusson and Hallgren [7, 8] and Magnusson et al. [9] studied several RC beams subject to blast loading in a shock tube. Liao et al. [10] presented the performance of high-strength RC beams under the explosion load. In this case, the pressure-impulse damage curves of RC beams were established using the maximum tensile reinforcement strain as a damage criterion. Multi-hazard approaches have also been developed in [11] considering the blast load after a fire and in [12] evaluating seismic design effects on the blast load resistance.

The performance prediction of structural systems subject to explosive blast loading has also received much attention. Among the initial contributions is the generalized single-degree-of-freedom (SDOF) representation of structural systems [13–20], a computationally convenient model with a simplified physics. The current approaches in blast design guidelines (e.g., [21]) widely use the generalized SDOF approximation. The literature also includes more nuanced representations of structural systems based on the beam theory [22], multi-degrees-of-freedom (MDOF), and Finite Element (FE) models [23–27]. The increasing computational capabilities and advances in numerical techniques have also enabled the seamless integration of blast load models, derived from first principles, with high-fidelity computational models of structural dynamics (see [28] for a review.)

33 However, the computational cost of high-fidelity models may limit their use in the reliability analysis of
34 structural systems with small failure probabilities. Therefore, current approaches for reliability analysis of
35 structural systems under blast loading (e.g., [20]) generally rely on simplified models, like the generalized
36 SDOF, to facilitate the failure probability estimation. For reliability analysis, these approaches usually
37 use sampling methods such as the Monte Carlo (MC) simulation and its several variants. However, these
38 approaches can be computationally intensive and often do not capture the effects of all the relevant sources
39 of uncertainty, including the compromises introduced in simplified structural models. Also, the developed
40 models are problem-specific that cannot generally be used for other, even similar systems. Finally, these
41 approaches do not fully exploit limited experimental data, often available at the structural component level
42 [27].

43 This paper proposes a physics-based probabilistic demand model and formulates the reliability for RC
44 beams under blast loading. The proposed model integrates the predicted demand from the governing equa-
45 tion of motion with an analytical correction term. The proposed formulation builds on a computationally
46 convenient model based on first principles. To this end, we first derive a generalized SDOF system from
47 the conservation law of energy, assuming smooth material constitutive laws and bending moment-curvature
48 relationship. We then develop an analytical correction term that captures discrepancies between the pre-
49 dicted deformation demand from the generalized SDOF system and the measured demand from available
50 experiments. The proposed demand model also includes a model error term that captures the remaining
51 uncertainty in model predictions. We use Bayesian inference to estimate the unknown model parameters in
52 the correction term and model error, combining predictions from the generalized SDOF system with exper-
53 imental data and any prior information. Similar formulations have been used to develop demand models
54 under other external stressors like impacts due to vehicle collision [29]. While in blast loading, a pressure
55 wave hits the structure, impact loading is the result of the collision of two or more bodies, producing a
56 loading condition characterized by high strain rates [30–32]. After discussing uncertainty classification, we
57 formulate the reliability problem using the developed probabilistic model. The use of smooth material con-
58 stitutive laws and bending moment-curvature relationship in the proposed formulation allows us to estimate
59 the failure probability using the First-Order Reliability Method (FORM). Compared with sampling methods,
60 FORM significantly reduces the computational cost of reliability analysis (i.e., reduces the number of system
61 evaluations from $\sim \mathcal{O}(10^5)$) in MC simulation method to $\sim \mathcal{O}(10)$) [33, 34]. At no additional cost, FORM
62 also provides the importance measures of random variables, which allow us to compare and rank random
63 variables based on their influence on the failure probability. To illustrate, we consider the reliability analysis
64 of an example RC beam subject to blast loading for three damage levels.

65 After this introduction, the rest of the paper is organized into four sections. Section 2 presents the

66 experimental dataset used to calibrate the proposed probabilistic demand model. Section 3 explains the
67 proposed physics-based probabilistic demand model for RC beams under blast loading. Section 4 discusses
68 the reliability analysis using the proposed probabilistic demand model. Finally, the last section summarizes
69 the paper and draws some conclusions.

70 2. Experimental Dataset

71 The laboratory experiments in [7–9] provide the database required to calibrate the proposed probabilistic
72 demand model. The database includes the responses of 21 simply supported RC beams subject to shock
73 waves produced by an air blast in a shock tube.

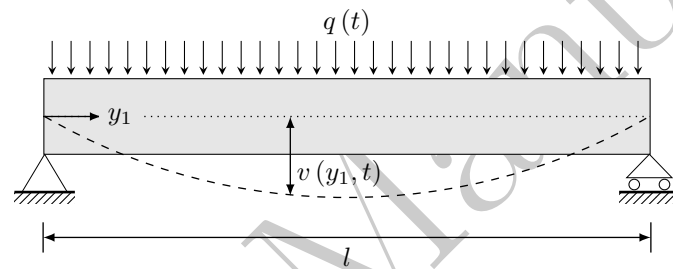


Figure 1: Boundary and loading conditions of a typical RC beam in the database

74

75 The explosive charge in the experiments was far enough from the beam to generate a plane wavefront,
76 resulting in a uniformly distributed load (see Figure 1). The prismatic RC beams in the database have a
77 span length of $l = 1.5$ m with a cross-section of depth $H = 0.16$ m and width $b = 0.3$ m. Table 1 summarizes
78 the relevant variables of the blast load and structural properties, and their range of values in the database.
79 The proposed probabilistic demand model is accurate for RC beams within the geometrical and mechanical
80 ranges summarized in Table 1. Unless the model is updated with new data, predictions outside the range
81 in Table 1 should be followed with caution as unseen factors, such as different reinforcements distribution
82 or geometrical and mechanical characteristics or geometrical and mechanical characteristics, may alter the
83 beam's global response and failure mode. In the next section, we explain model updating with new data.

84

85 3. Proposed Physics-based Probabilistic Demand Model

86 This section presents the proposed physics-based probabilistic model. The section first reviews a general
87 formulation for developing a probabilistic demand model [35–37], followed by a Bayesian parameter estima-

Table 1: Range of the values of the blast load and structural variables in the database

Variable	Symbol	Range
Equivalent TNT mass [kg]	Q	1.24-4.96
Scaled distance [$\text{m}/\text{kg}^{1/3}$]	z	6.05-24.19
Reflected peak pressure [kPa]	P_r	650-1,957
Positive phase duration [msec]	t_d	16-36
Impulse [kPa-sec]	I	3.76-11.54
RC specific weight [kN/m^3]	ρ	24.3-29.4
Concrete compressive strength [MPa]	f_{cu}	43-173
Ultimate concrete strain [%]	ε_{cu}	0.28 -0.35
Reinforcement yielding strength [MPa]	f_{sy}	544-604
Reinforcement ratio [%]	ρ_s	1.21-2.75
Beam yielding midspan displacement [mm]	v_y	7.1-10.5
Beam ultimate midspan displacement [mm]	v_u	11.6-16.4

tion [38] and model selection [35]. We then use the general formulation to develop the proposed probabilistic deformation demand model for RC beams subject to blast loads.

3.1. Formulation of the probabilistic model

Formulating a physics-based probabilistic demand model starts with predicting the demand measure from the governing differential equation. For computational efficiency, the governing differential equation may represent the simplified physics of a more complex phenomenon. We then introduce a correction term to capture the mismatch between the actual demand value and that predicted from the differential equation. Mathematically, we write the physics-based probabilistic demand model as [35–37]

$$T[D(\mathbf{x}, \Theta)] = T[\hat{d}(\mathbf{x})] + \gamma(\mathbf{x}, \theta) + \sigma\varepsilon, \quad (1)$$

where $T(\cdot)$ is a transformation function; $D(\mathbf{x}, \Theta) = \Delta(\mathbf{x}, \Theta)/l$ is the non-dimensional demand in this paper, in which $\Delta(\mathbf{x}, \Theta)$ is the predicted deformation demand; $\hat{d}(\mathbf{x}) = \hat{\delta}(\mathbf{x})/l$, in which $\hat{\delta}(\mathbf{x})$ is the predicted deformation demand from the governing differential equation; $\gamma(\mathbf{x}, \theta)$ is the correction term; \mathbf{x} is the vector of state variables, such as material properties, characteristics of external stressors, boundary and initial conditions, and geometry; $\Theta = (\theta, \sigma)$ is the vector of unknown model parameters that need to be estimated; and $\sigma\varepsilon$ is an additive model error (additivity assumption), in which σ is the standard deviation of the model error, assumed not to depend on \mathbf{x} (homoskedasticity assumption), and ε is a standard normal random variable (normality assumption). Diagnostic plots [39] can guide the selection of an appropriate $T(\cdot)$ to (approximately) satisfy the additivity, homoskedasticity, and normality assumptions over the range of the data. Furthermore, Box and Cox [40] proposed a parameterized family of transformations that provide the possible choices for $T(\cdot)$.

Following [35], we write the analytical correction term as

$$\gamma(\mathbf{x}, \boldsymbol{\theta}) = \sum_{k=1}^{N_h} \theta_k h_k(\mathbf{x}), \quad (2)$$

where $\boldsymbol{\theta} = (\theta_1, \dots, \theta_{N_h})$ and $h_k(\mathbf{x})$, $k = 1, \dots, N_h$, are explanatory functions. Mathematically, the explanatory functions form the bases of function space to model the variabilities of $T(D)$ not explained by the differential equation. The physical interpretation is that the explanatory functions capture the aspects of the governing physical laws that are compromised in the differential equation [37].

3.2. Bayesian parameter estimation and model selection

Once the probabilistic model is formulated, we use the database introduced in Section 2 to estimate Θ . Using Bayesian inference, we integrate the information from the experimental data with any prior information about Θ . To estimate Θ , we use the Bayes theorem [38]

$$f(\Theta) = \kappa L(\Theta) p(\Theta), \quad (3)$$

where $f(\Theta)$ is the posterior distribution that represents the updated information about Θ ; $L(\Theta)$ is the likelihood function that includes the objective information from the experimental data; $p(\Theta)$ is the prior distribution that represents the information available before collecting the experimental data; and $\kappa = [\int L(\Theta) p(\Theta) d\Theta]^{-1}$ is a normalizing constant.

To write $L(\Theta)$, following [35], we first partition the data into equality data \mathcal{D}_{eq} if the measured values of deformation demand are the actual values, and lower bound data (or censored data) \mathcal{D}_{lb} , if the measured values are less than the actual ones. For example, in a failed or interrupted test, the largest recorded value during the test serves as a lower bound of the actual demand value for that test. Otherwise, the recorded value would represent the actual demand value. We then write $L(\Theta)$ as

$$L(\Theta) \propto \mathbb{P} \left\{ \bigcap_{i:D_i \in \mathcal{D}_{eq}} [r_i(\boldsymbol{\theta}) = \sigma\varepsilon] \bigcap_{i:D_i \in \mathcal{D}_{lb}} [r_i(\boldsymbol{\theta}) < \sigma\varepsilon] \right\}, \quad (4)$$

where $r_i(\boldsymbol{\theta}) = T[D_i] - T[\hat{d}(\mathbf{x}_i)] - \gamma(\mathbf{x}_i, \boldsymbol{\theta})$ is the value of the model error (or the residual) for the i th datum. For statistically independent residuals, we can write $L(\Theta)$ as

$$L(\Theta) \propto \prod_{i:D_i \in \mathcal{D}_{eq}} \frac{1}{\sigma} \phi \left[\frac{r_i(\boldsymbol{\theta})}{\sigma} \right] \prod_{i:D_i \in \mathcal{D}_{lb}} \Phi \left[-\frac{r_i(\boldsymbol{\theta})}{\sigma} \right], \quad (5)$$

where $\phi(\cdot)$ and $\Phi(\cdot)$ are the standard Normal probability density and distribution functions. The prior distribution $p(\Theta)$ can incorporate any additional information about Θ available before using the data to

129 construct $L(\Theta)$. In the absence of additional information, we may simply use a noninformative prior
130 distribution as $p(\Theta) \propto 1/\sigma$ [35].

131 The computation of the posterior distribution requires evaluating the normalizing constant κ in Eq.
132 (3), which often entails an analytically intractable integral. However, we may sample from the posterior
133 distribution by simulating a Markov Chain whose stationary distribution is $f(\Theta)$. In this paper, we use
134 an adaptive, delayed-rejection algorithm [41] to construct the Markov Chain. To accelerate the Markov
135 Chain's convergence, we construct its transition (or proposal) density based on the Gaussian approximation
136 of the posterior distribution. Specifically, we construct the covariance matrix of the transition density as
137 $-\left[\nabla\nabla\ln L(\Theta)\right]^{-1}$, evaluated at the maximum likelihood estimate of Θ [42]. We also use the maximum
138 likelihood estimate of Θ as the initial state of the Markov Chain.

139 The inclusion of insignificant terms in $\gamma(\mathbf{x}, \theta)$ may lead to increased model uncertainty and over-fitting
140 the data. To develop a parsimonious (simple yet accurate) form of $\gamma(\mathbf{x}, \theta)$, we follow a stepwise deletion
141 process developed in [35] for regression analysis with censored data. We begin with the complete form of
142 $\gamma(\mathbf{x}, \theta)$ and successively eliminate one $h_k(\mathbf{x})$ at a time, based on the posterior Coefficients of Variation
143 (CoV) of each θ . After each elimination, we re-calibrate the remaining Θ . The stopping criterion of the
144 elimination process is based on the balance between the desired level of model accuracy, captured by σ ,
145 and model simplicity. Furthermore, we may combine strongly correlated parameters θ_{k_1} and θ_{k_2} (e.g., with
146 $|\rho_{k_1, k_2}| \gtrsim 0.7$) in the final form of $\gamma(\mathbf{x}, \theta)$ as [35]

$$\hat{\theta}_{k_1} = \mu_{k_1} + \rho_{k_1, k_2} \sigma_{k_1} \frac{\theta_{k_2} - \mu_{k_2}}{\sigma_{k_2}}, \quad (6)$$

147 where μ_{k_1} and σ_{k_1} are the posterior mean and standard deviation of θ_{k_1} , and θ_{k_1} has the higher CoV of the
148 two parameters.

149 3.3. Proposed probabilistic demand model for RC beams under blast loads

150 We now use the general formulation in Eq. (1) to develop the proposed probabilistic deformation demand
151 model. We first formulate $\hat{\delta}(\mathbf{x})$ by deriving the differential equation that governs the dynamics of the RC
152 beam (i.e., the generalized SDOF representation of the beam model.) We then design the correction term
153 $\gamma(\mathbf{x}, \theta)$ and calibrate the probabilistic model with the experimental data introduced in Section 2.

154 3.3.1. Deterministic model

155 We invoke the conservation law of energy to derive the governing differential equation. The conservation
156 of energy requires that the external work W done on the beam being in balance with the sum of kinetic K
157 and strain U energies of the beam at any time instant t . i.e.,

$$W(t) = K(t) + U(t). \quad (7)$$

158 The external work done by a general load q is

$$W(t) = \int_0^t \int_0^l q(y_1, \tau) \frac{\partial v(y_1, \tau)}{\partial \tau} dy_1 d\tau, \quad (8)$$

159 where y_1 is the longitudinal coordinate; and v is the transverse displacement as shown in Figure 1. Following

160 Freidlander [43], we write the uniform blast time-history $q(y_1, t) \equiv q(t)$ as

$$q(t) = bP_r (1 - t/t_d) e^{-2t/t_d}, \quad (9)$$

161 where P_r is the reflected pressure peak; and t_d is the phase duration. Following [44], we obtain P_r from

$$\begin{aligned} P_r &= 2P_{so} \left(\frac{7P_{atm} + 4P_{so}}{7P_{atm} + P_{so}} \right), \\ P_{so} &= 1.772/z^3 - 0.114/z^2 + 0.108z, \\ z &= R/W^{1/3}, \end{aligned} \quad (10)$$

162 where $P_{atm} = 0.1$ MPa is the atmospheric pressure; P_{so} is the stand-off pressure that is obtained from the
163 Mills' model [45]; z is the scaled distance from the explosive charge; R is the distance between the beam and
164 explosive charge; and W is the explosive charge in [kg] of equivalent TNT.

165 Assuming a triangular impulse, we then obtain t_d from

$$\begin{aligned} t_d &= 2I_{so}/P_{so}, \\ I_{so} &= cW^{2/3}/R, \end{aligned} \quad (11)$$

166 where I_{so} is the incident impulse according to Held's equation [46]; c is a numerical coefficient equal to
167 4.8×10^5 in this work, following the information reported in [47, 48].

168 Next, we express the kinetic energy as

$$K(t) = \int_0^l \frac{1}{2} \mu \left[\frac{\partial v(y_1, t)}{\partial t} \right]^2 dy_1, \quad (12)$$

169 where μ is the mass per unit length. Finally, we express the strain energy as

$$U(t) = \int_0^l \int_0^{\varphi(y_1, t)} M(\varphi) d\varphi dy_1, \quad (13)$$

170 where $M(\varphi)$ is the developed bending moment in the beam, which is a function of curvature $\varphi \in [0, \varphi(y_1, t)]$;
 171 and $\varphi(y_1, t)$ is the curvature of the beam at location y_1 and time t . Following [22] and [14], we use a smooth
 172 bending moment-curvature relationship (see Figure 2) as

$$M(\varphi) = \bar{M} \tanh\left(\frac{\bar{K}}{\bar{M}}\varphi\right) = -\bar{M} \tanh\left(\frac{\bar{K}}{\bar{M}}\frac{\partial^2 v}{\partial y_1^2}\right), \quad (14)$$

173 where \bar{M} is the equivalent ultimate bending moment (see Figure 2); $\bar{K} = M_y/\varphi_y$ is the slope of the elastic
 174 regime, in which M_y and φ_y are the yield moment and curvature; and $\varphi = -\partial^2 v/\partial y_1^2$. Substituting Eq. (14)
 175 into Eq. (13) then yields

$$U(t) = \int_0^l \frac{\bar{M}^2}{\bar{K}} \ln \left[\cosh \left(-\frac{\bar{K}}{\bar{M}} \frac{\partial^2 v}{\partial y_1^2} \right) \right] dy_1, \quad (15)$$

176 where \bar{M} is obtained by equating the area under the derived bilinear curve A_1 (i.e., its strain energy) with
 177 that of the hyperbolic curve A_2 (see Figure 2). Next, we explain the derivation of the bilinear curve from
 178 cross-section analysis.

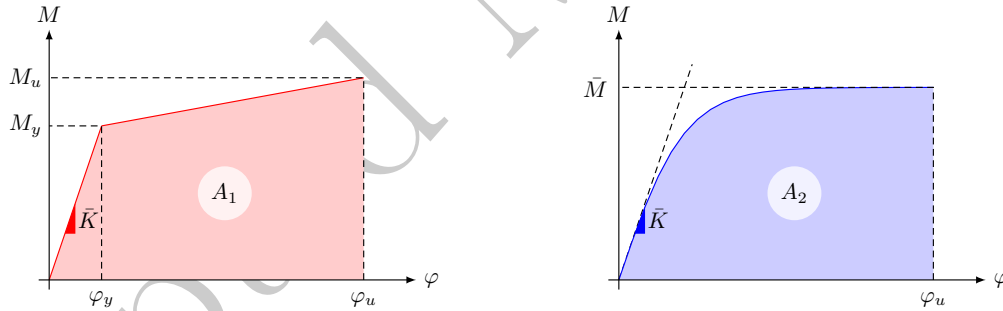


Figure 2: Section bending moment-curvature diagrams

179

180 The section arrives at its yield state when the strain in the tensile reinforcement $\bar{\epsilon}_s$ reaches the yield
 181 strain $\bar{\epsilon}_{sy}$. The respective neutral axis depth is c_y (see Figure 3). We obtain c_y and M_y from the section
 182 equilibrium at the yield state as

$$\begin{aligned} b \int_0^{c_y} \bar{\sigma}_c dy_2 + \bar{\sigma}_{ss} A_{ss} &= f_{sy} A_s, \\ b \int_0^{c_y} \bar{\sigma}_c (d - y_2) dy_2 + \bar{\sigma}_{ss} A_{ss} (d - d') &= M_y, \end{aligned} \quad (16)$$

183 where $\bar{\sigma}_c = \bar{\sigma}_c(y_2)$ is the developed compressive stress in the concrete at depth y_2 ; $\bar{\sigma}_{ss}$ is the developed
 184 stress in the compressive reinforcement; f_{sy} is the yield stress of the tensile reinforcement; A_s is the total

185 cross-section area of the tensile reinforcements; and A_{ss} is the total cross-section area of the compressive
 186 reinforcements. Accordingly, we obtain the yield curvature from geometry as $\varphi_y = \bar{\epsilon}_{sy} / (d - c_y)$ (see Figure
 187 3), where d is the depth of tensile reinforcements.

188 The section arrives at its ultimate state when the strain in the concrete's extreme compressive fiber
 189 reaches $\bar{\epsilon}_{cu}$, and the strain in the tensile reinforcement exceeds $\bar{\epsilon}_{sy}$. The respective neutral axis depth is c_u
 190 (see Figure 3). We obtain c_u and M_u from the section equilibrium at the ultimate state as

$$b \int_0^{c_u} \bar{\sigma}_c dy_2 + \bar{\sigma}_{ss} A_{ss} = f_{sy} A_s, \quad (17)$$

$$b \int_0^{c_u} \bar{\sigma}_c (d - y_2) dy_2 + \bar{\sigma}_{ss} A_{ss} (d - d') = M_u,$$

191 and the respective curvature from geometry is $\varphi_u = \bar{\epsilon}_{cu} / c_u$ (see Figure 3). The pairs (M_y, c_y) and (M_u, c_u)
 192 completely characterize the bilinear bending moment-curvature diagram, shown in Figure 2.

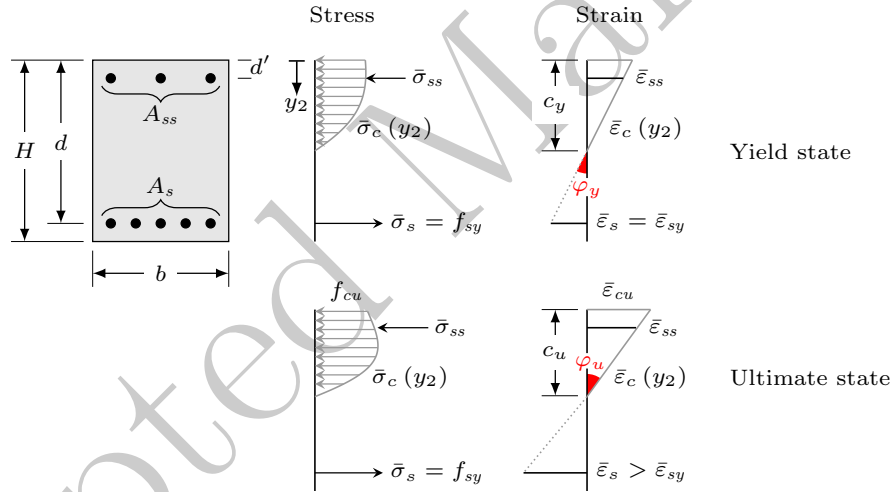


Figure 3: Stress and strain distributions over the cross-section in yield and ultimate states

193

194 The calculation of (M_y, c_y) and (M_u, c_u) from Eqs. (16) and (17) requires specifying the material con-
 195 stitutive laws (i.e., stress-strain relationships). Following [48], we represent the stress-strain relationship
 196 of reinforcing steel, both in tension and compression, by an elastic-plastic model. Also, we express the
 197 stress-strain relationship of concrete in compression as

$$\bar{\sigma}_c = \frac{f_{cc} [k \bar{\epsilon}_c / \bar{\epsilon}_{cc} - (\bar{\epsilon}_c / \bar{\epsilon}_{cc})^2]}{1 + (k-2) \bar{\epsilon}_c / \bar{\epsilon}_{cc}}, \quad |\bar{\epsilon}_c| < |\bar{\epsilon}_{cu}|, \quad (18)$$

198 where $f_{cc} (< 0)$ is the compressive strength of concrete; $\bar{\epsilon}_{cc} (< 0)$ is the respective compressive strain; and k
 199 is the plasticity number. This model neglects the tension strength of concrete.

200 We further capture the strain rate effects on steel and concrete behavior due to the dynamic blast loading.
201 Specifically, following [47], we write the dynamic compressive strength of concrete $f_{cc,dyn}$ as

$$f_{cc,dyn} = \begin{cases} f_{cc} [\dot{\bar{\epsilon}}_c / (30 \times 10^{-6})]^{1.026\alpha_c}, & \dot{\bar{\epsilon}}_c \leq 30, \\ f_{cc}\eta\dot{\bar{\epsilon}}_c^{1/3}, & \dot{\bar{\epsilon}}_c > 30, \end{cases} \quad (19)$$

202 where $\dot{\bar{\epsilon}}_c$ [s⁻¹] is the concrete strain rate, with $\alpha_c = 1 / (5 + 0.75f_{cc})$ and $\eta = 10^{6.156\alpha_c - 0.492}$. We also capture
203 the strain rate effects on $\bar{\epsilon}_{cc}$ and $\bar{\epsilon}_{cu}$ as [47]

$$\begin{aligned} \bar{\epsilon}_{cc,dyn} &= \bar{\epsilon}_{cc} [\dot{\bar{\epsilon}}_c / (30 \times 10^{-6})]^{0.02}, \\ \bar{\epsilon}_{cu,dyn} &= \bar{\epsilon}_{cu} [\dot{\bar{\epsilon}}_c / (30 \times 10^{-6})]^{0.02}, \end{aligned} \quad (20)$$

204 where $\bar{\epsilon}_{cc,dyn}$ is the dynamic strain of concrete corresponding to $f_{cc,dyn}$; and $\bar{\epsilon}_{cu,dyn}$ is the dynamic ultimate
205 strain of concrete. Finally, we write the dynamic yielding strength of steel $f_{sy,dyn}$ as [47]

$$f_{sy,dyn} = f_{sy} \left[1 + \frac{6}{f_{sy}} \ln \left(\frac{\min \{\dot{\bar{\epsilon}}_s, 10\}}{50 \times 10^{-6}} \right) \right], \quad (21)$$

206 where $\dot{\bar{\epsilon}}_s$ [s⁻¹] is the steel strain rate.

207 In summary, we rewrite the conservation law of energy in Eq. (7) in the form of an integro-differential
208 equation

$$\int_0^l \left\{ \frac{1}{2} \mu \left(\frac{\partial v}{\partial t} \right)^2 + \frac{\bar{M}^2}{\bar{K}} \ln \left[\cosh \left(-\frac{\bar{K}}{\bar{M}} \frac{\partial^2 v}{\partial y_1^2} \right) \right] - \int_0^t q(\tau) \frac{\partial v}{\partial \tau} d\tau \right\} dy_1 = 0, \quad (22)$$

209 supplemented by the materials' constitutive laws, and subject to the boundary conditions $v(y_1 = 0, \tau) =$
210 $v(y_1 = l, \tau) = 0$, for $\tau \in (0, t]$, and the initial condition $v(y_1, \tau = 0) = 0$, for $y_1 \in (0, l)$.

211 Following [49], we represent the trial functions using the spectral expansion

$$v(y_1, t) = \sum_{j=1}^{\infty} V_j(t) \sin[(2j-1)\pi y_1/l], \quad (23)$$

212 where $V_j(t)$'s are the unknown spectral functions that need to be estimated. The functional form of the trial
213 functions readily satisfies the boundary conditions, and the underlying symmetry of the problem.

214 To facilitate the computation of $v(y_1, t)$, we only retain the first term of the trial functions in Eq. (23) and
215 capture the effects of this approximation by the correction term (see Eq. 1). Furthermore, Cox et al. [49] have
216 shown that the error incurred in approximating the maximum strain energy by retaining only the first term
217 is less than 3% of the approximation with the first two terms. Then, substituting $v(y_1, t) \cong V_1(t) \sin(\pi y_1/l)$

218 into Eq. (22) yields

$$\frac{\mu l}{4} \left(\frac{dV_1}{dt} \right)^2 + \frac{\bar{M}^2}{\bar{K}} \int_0^l \ln \left\{ \cosh \left[\frac{\bar{K}}{\bar{M}} \frac{\pi^2}{l^2} V_1 \sin \left(\frac{\pi}{l} y_1 \right) \right] \right\} dy_1 - \frac{2l}{\pi} \int_0^t q(\tau) \frac{dV_1}{d\tau} d\tau = 0. \quad (24)$$

219 We use a second-order central finite-difference scheme to transform the integro-differential equation into
220 the following algebraic equation in only unknown $V_1(t)$:

$$\begin{aligned} \frac{\mu l}{4} \left(\frac{V_{1,n_t+1} - V_{1,n_t-1}}{2\Delta\tau} \right)^2 + \frac{\bar{M}^2}{\bar{K}} \sum_{m=1}^{m_s+1} \ln \left\{ \cosh \left[\frac{\bar{K}}{\bar{M}} \frac{\pi^2}{l^2} V_{1,n_t} \sin \left(\frac{\pi}{l} y_{1,m} \right) \right] \right\} \Delta y_1 \\ - \frac{2l}{\pi} \sum_{n=1}^{n_t} q_n \frac{V_{1,n+1} - V_{1,n-1}}{2\Delta\tau} \Delta\tau = 0, \end{aligned} \quad (25)$$

221 where $\Delta\tau$ and Δy_1 are the space and time increments; n is the time index, and m is the space index; and
222 $n_t + 1$ and $m_s + 1$ are the total number of time and space increments. We solve this equation sequentially
223 for each time step. Algorithm 1 summarizes the implementation of Eq. (25).

Algorithm 1 Second-order central finite-difference scheme to solve for $V_1(t)$

- 1: set the time horizon
 - 2: set the space and time increments $\Delta\tau$ and Δy_1
 - 3: set the total number of space and time increments $N_t \leftarrow \lceil t/\Delta\tau \rceil$ and $N_s \leftarrow \lceil l/\Delta y_1 \rceil$
 - 4: initialize the unknown function $V_{1,0} \leftarrow 0$
 - 5: **for** n_t **from** 1 **to** N_t **do**
 - 6: compute the unknown $V_{1,n_t+1} \leftarrow$ Solve Eq. (25)
 - 7: compute the curvature at midspan $\varphi \leftarrow -\partial^2 v / \partial y_1^2 = \pi^2 / l^2 V_{1,n_t+1}$
 - 8: compute the curvature rate $\dot{\varphi} = \partial\varphi / \partial t \leftarrow (V_{1,n_t+1} - V_{1,n_t-1}) / (2\Delta\tau)$
 - 9: compute the respective bending moment $M(\varphi) \leftarrow \bar{M} \tanh(\bar{K} / \bar{M} \varphi)$
 - 10: compute the neutral axis depth $c \leftarrow$ Solve $[b \int_0^c \bar{\sigma}_c (d - y_2) dy_2 + \bar{\sigma}_{ss} A_{ss} = M]$
 - 11: compute the strains in extreme concrete fiber $\bar{\varepsilon}_c \leftarrow c \tan(\varphi)$
 - 12: compute the strains in compression and tension steel fibers $\bar{\varepsilon}_{ss} \leftarrow (c - d') \tan(\varphi)$; $\bar{\varepsilon}_s \leftarrow (d - c)$
 - 13: adjust the material properties for the strain rate effects using Eqs. (19)-(21)
 - 14: update the mechanical properties of the section c_y, M_y, c_u, M_u using Eq. (16) and (17)
 - 15: update $\bar{K} \leftarrow M_y / \varphi_y$ and $\bar{M} \leftarrow$ Solve $\{\bar{M} / \bar{K} \ln [\cosh(\bar{M} / \bar{K} \varphi_u)] = 0.5 [M_u (\varphi_u - \varphi_y) + M_y \varphi_u]\}$
 - 16: **if** $\varphi \geq \varphi_u$ **then**
 - 17: | break
 - 18: **end if**
 - 19: **end for**
 - 20: Output $\leftarrow V_{1,1:N_t+1}$
-

224 Finally, we express the deterministic deformation demand as

$$\begin{aligned}
 \hat{\delta}(\mathbf{x}) &= \sup_{\tau \in [0, t]} \max_{y_1 \in (0, l)} v(y_1, \tau) \\
 &= \sup_{\tau \in [0, t]} V_1(\tau),
 \end{aligned} \tag{26}$$

where $\max_{y_1 \in (0, l)} v(y_1, \tau) = V_1(\tau)$ follows from the embedded symmetry in the problem.

3.3.2. Model correction

In this section, we design the correction term (see Eq. 2) to capture the physical characteristics not fully represented by $\hat{d}(\mathbf{x}) = \hat{\delta}(\mathbf{x})/l$. As the candidate explanatory functions, we define $h_1(\mathbf{x}) = 1$ to capture a potential constant bias in the model $\hat{d}(\mathbf{x})$; $h_2(\mathbf{x}) = \varphi_y H$ and $h_3(\mathbf{x}) = \varphi_u H$ to consider the beam's flexural characteristics; $h_4(\mathbf{x}) = \bar{\varepsilon}_{cu}$, $h_5(\mathbf{x}) = f_{sy}/f_{cu}$, and $h_6(\mathbf{x}) = \rho_s f_{sy}/f_{cu}$ to consider the materials' mechanical characteristics; and, $h_7(\mathbf{x}) = z/z_{max}$ and $h_8(\mathbf{x}) = P_r/P_{r,max}$ to consider the load characteristics, where z_{max} and $P_{r,max}$ are the maximum values of the scaled distance and reflected pressure peak in the experimental dataset. All the explanatory functions are non-dimensional, and their selections are aimed at capturing the aspects of beams behavior not fully represented by the deterministic model.

3.3.3. Parameter estimation and model selection

In this section, we shorten the list of explanatory functions in $\gamma(\mathbf{x}, \boldsymbol{\theta})$ to obtain a parsimonious model. Figure 4 shows the posterior CoV of θ_k 's (with dots) and the posterior mean of σ (with open squares) at each step in the deletion process. We stop the deletion process at Step 7, retaining $\theta_3 h_3(\mathbf{x})$ and $\theta_4 h_4(\mathbf{x})$ in the final form of the model.

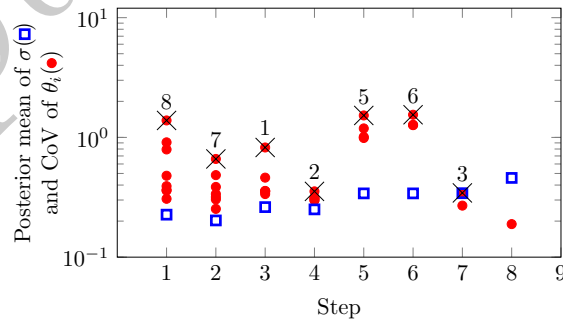


Figure 4: Stepwise deletion process of the deformation demand model

Table 2 summarizes the posterior statistics of $\Theta = (\theta_3, \theta_4, \sigma)$. The obtained results indicate that θ_3 and θ_4 are highly correlated; hence, we combine them using Eq. (6), resulting in a correction term with only one parameter as

$$\gamma(\mathbf{x}, \boldsymbol{\theta}) = \theta_3 \varphi_u H + (0.1107 - 0.6189\theta_3) \bar{\epsilon}_{cu}. \quad (27)$$

243 The negative mean of θ_3 indicates that $\hat{d}(\mathbf{x})$ generally tends to overestimate the contribution of ultimate
 244 curvature, whereas the positive mean of θ_4 indicates that $\hat{d}(\mathbf{x})$ tends to underestimate the contribution of
 245 concrete ultimate strain. However, Eq. (27) should not be interpreted in a mechanistic way in explaining
 246 the role of each explanatory functions; the values of the parameters simply provide a good fit to the data
 247 [50, 51].

Table 2: Posterior statistics of parameters in the deformation demand model

Parameter	Mean	Standard deviation	Correlation coefficient		σ
			θ_3	θ_4	
θ_3	-0.628	0.216	1	-0.994	0.11
θ_4	0.499	0.134	-0.994	1	-0.1285
σ	0.342	0.075	0.11	-0.1285	1

248 Figure 5 shows a comparison between the measured and predicted non-dimensional deformation demands
 249 (i.e., $D = \Delta/l$) of all the beams in the database. The predictions are according to the deterministic (left plot)
 250 and probabilistic (right plot) models. For a perfect model, the equality data \mathcal{D}_{eq} should line up along the 1:1
 251 solid line and the lower-bound data \mathcal{D}_{lb} should lie above the 1:1 line. The predictions from the generalized
 252 SDOF representation (i.e., deterministic model) tend to overestimate the demand. The proposed probabilistic
 253 model effectively corrects the bias in the generalized SDOF representation. The predicted equality data are
 254 evenly spread around the 1:1 line, mostly within the dashed lines defined as $\pm\sigma$ away from the 1:1 line. Also,
 255 almost all the lower-bound data are still above the 1:1 line.

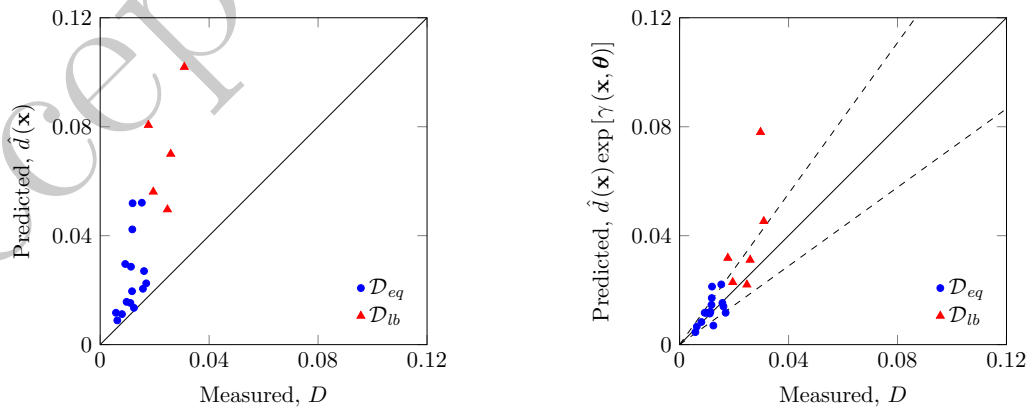


Figure 5: Comparison between measured and predicted deformation demand based on deterministic (left) and probabilistic (right) models

256

257 *Remark.* The number of training data required to estimate the unknown model parameters Θ mainly depends
258 on the complexity of the relation between the system demand D and its state variables \mathbf{x} (i.e. the number
259 of unknown parameters). A database with 21 training data, used in this paper, might generally be small for
260 developing a data-driven probabilistic demand model. However, developing physics-based probabilistic models
261 (like we do in this paper) requires fewer data. The level of dependence on (experimental) data is reduced
262 by incorporating available knowledge in various forms, including existing (deterministic) models based on
263 first principles, informative explanatory functions, and informative prior distributions on Θ . Specifically, we
264 could develop a relatively simple yet accurate probabilistic demand model with only two parameters (θ_3, σ)
265 by incorporating first principles and informative explanatory functions. In addition, as more data become
266 available in the future, the model can be updated using Bayesian inference (see Eq. 3).

267 4. Reliability Analysis using the Proposed Physics-based Probabilistic Model

268 Reliability analysis aims to estimate the probability that a system fails to satisfy its intended design
269 purposes. The evaluation of failure probability requires characterizing the sources of uncertainty and quan-
270 tifying their effects on the system's responses. This section first explains the sources of uncertainty in the
271 proposed physics-based probabilistic demand model, followed by the formulation of the reliability problem,
272 and the treatment of different uncertainties in the reliability analysis. Finally, we conduct the reliability
273 analysis of an example RC beam subject to blast loading.

274 4.1. Uncertainty classification

275 The proposed physics-based probabilistic demand model involves various sources of uncertainty that need
276 to be characterized and properly treated in the reliability analysis. Following [35], we categorize these sources
277 of uncertainty into four groups. First, there is inherent uncertainty in state variables \mathbf{x} . We capture the
278 uncertainty in \mathbf{x} by a parameterized probability density function $f(\mathbf{x}, \boldsymbol{\theta}_f)$, where $\boldsymbol{\theta}_f$ is a vector of distribution
279 parameters. The choice of the model for $f(\mathbf{x}, \boldsymbol{\theta}_f)$ is itself a source of uncertainty that mainly affects the
280 reliability analysis of systems with small failure probability. As a particular case, this uncertainty might be
281 limited to the uncertainty in the distribution parameters [52]. Second, the model error $\sigma\varepsilon$ is another source
282 of uncertainty (i.e., model uncertainty) that captures the collective effects of missing variables, the selected
283 mathematical form of the probabilistic demand model, and numerical error of the finite-difference solution.
284 Third, there is statistical uncertainty in the estimation of the unknown parameters using the experimental
285 data. The unknown parameters can include both the model parameters Θ and the distribution parameters
286 $\boldsymbol{\theta}_f$. In general, the posterior distribution from the Bayesian inference is intended to capture the statistical
287 uncertainty in Θ and $\boldsymbol{\theta}_f$. In the rest of this section we treat $\boldsymbol{\theta}_f$ as a deterministic parameter; though, its

288 treatment in the reliability analysis is similar to that of Θ . Finally, the model parameters are estimated
289 from the experimental data that may include measurement errors from measurement devices or procedures
290 inaccuracy. The treatment of this uncertainty in the development of probabilistic models can be found in
291 [35, 53].

292 *4.2. Reliability analysis using the proposed physics-based probabilistic model*

293 Mathematically, we represent the failure event by defining a limit-state function $g(\mathbf{x}, \Theta)$ as [33, 34]

$$g(\mathbf{x}, \Theta) = C - D(\mathbf{x}, \Theta), \quad (28)$$

294 where C is the capacity estimate. We obtain the non-dimensional capacity $C = v_{max}/l$ from its geometrical
295 relationship with the beam's end rotation angle through $C \cong \frac{\tan \alpha}{2}$, where v_{max} is the midspan maximum
296 deformation and α is the respective beam's end rotation angle. Table 3 shows the thresholds of α associated
297 with different damage levels [54]. We note that the capacity and demand models of a system generally share
298 the same input random variables that represent system characteristics. However, their levels of uncertainty
299 may not necessarily be comparable. The reason is that the model error is often the dominant source of
300 uncertainty that can significantly differ between the capacity and demand models (we will explain this point
301 later in the numerical example.) With comparable levels of model refinement, the demand model is usually
302 more uncertain than the corresponding capacity model due to the uncertainty in the intensity measures of
303 external stressors that go into the demand model. Thus, as the first step, we focused on the demand model
304 herein and developing the capacity model remains a subject for future research.

Table 3: Capacity thresholds associated with different damage levels

Damage level	Rotation α [deg]
Moderate	≤ 2
Heavy	≤ 5
Blowout	≤ 10

305 For a given Θ , the failure probability $P_F(\Theta)$ and reliability index $\beta(\Theta)$ are obtained from

$$P_F(\Theta) = \int_{\Omega_F(\Theta)} f(\mathbf{x}) \phi(\varepsilon) d\mathbf{x}d\varepsilon, \quad (29)$$

$$\beta(\Theta) = \Phi^{-1}[1 - P_F(\Theta)],$$

306 where $\Omega_F(\Theta)$ is the failure event, defined as $\Omega_F(\Theta) = \{(\mathbf{x}, \varepsilon) : g(\mathbf{x}, \Theta) \leq 0\}$. The estimation of the failure
307 probability accounts for the uncertainty in the state variables and model uncertainty. As discussed in [35],
308 one can also include the uncertainty from measurement errors in the computation of the failure probability.

309 In reliability theory, it is common to compute P_F by first evaluating the conditional failure probability
310 (i.e., fragility) as a function of the intensity measures of external stressors (i.e., the scaled distance z herein)
311 [35, 55]. Mathematically, we express the fragility function as

$$F(z, \Theta) = \int_{\Omega_F(z, \Theta)} f(\mathbf{r}, z) \phi(\varepsilon) \, d\mathbf{r} d\varepsilon, \quad (30)$$

312 where \mathbf{x} is partitioned as $\mathbf{x} = (\mathbf{r}, z)$, in which \mathbf{r} contains the characteristics of the system (e.g., material
313 properties and geometry); and $\Omega_F(z, \Theta)$ is the failure event for a given value of z . We then obtain the
314 fragility function (i.e., evaluate Eq. 30) from reliability analyses for different values of z [33]. To capture the
315 effects of statistical uncertainty in Θ , we compute the predictive estimate of the fragility function as [35]

$$\begin{aligned} \tilde{F}(z) &= \mathbb{E}_{\Theta} [F(z, \Theta)] \\ &= \int F(z, \Theta) f(\Theta) \, d\Theta, \end{aligned} \quad (31)$$

316 where $\mathbb{E}_{\Theta} [F(z, \Theta)]$ is the expected value of $F(z, \Theta)$ with respect to Θ , and $f(\Theta)$ is the posterior distribution
317 of Θ from Bayesian inference. The confidence interval of $\tilde{F}(z)$ is then

$$[\Phi(-\tilde{\beta}(z) - \sigma_{\beta}(z)), \Phi(-\tilde{\beta}(z) + \sigma_{\beta}(z))], \quad (32)$$

318 where $\tilde{\beta}(z) = \Phi^{-1} [1 - \tilde{F}(z)]$ is the generalized reliability index, and

$$\sigma_{\beta}(z) \cong \nabla_{\Theta} \beta(z) \Sigma_{\Theta\Theta} \nabla_{\Theta}^T \beta(z), \quad (33)$$

319 is the variance of the reliability index, obtained from the first-order Taylor expansion around the posterior
320 mean of Θ . The confidence interval is approximately the interval between 0.15 and 0.85 quantiles, see [35].

321 To systematically identify the critical sources of uncertainty, we compute the importance measures of
322 random variables $\mathbf{y} = (\mathbf{x}, \varepsilon, \Theta)$ as [56]

$$\gamma = \frac{\alpha \mathbf{J}_{\mathbf{u}^*, \mathbf{y}^*} \check{\mathbf{D}}}{\|\alpha \mathbf{J}_{\mathbf{u}^*, \mathbf{y}^*} \check{\mathbf{D}}\|}, \quad (34)$$

323 where γ is the vector of importance measures in the original probability space; $\alpha = -\nabla G(\mathbf{u}^*) / \|\nabla G(\mathbf{u}^*)\|$
324 is the vector of importance measures in the standard Normal probability space; $\|\cdot\|$ is the Euclidean norm;
325 \mathbf{u}^* is the most likely failure point in the standard Normal probability space, called the design point; \mathbf{y}^*
326 is the counterpart of \mathbf{u}^* in the original probability space; $G(\mathbf{u}^*) = g[\mathbf{T}(\mathbf{y}^*)]$, in which $\mathbf{T} : \mathbf{y} \rightarrow \mathbf{u}$ is an
327 injective mapping from the original to standard Normal probability space; $\mathbf{J}_{\mathbf{u}^*, \mathbf{y}^*} = \nabla_{\mathbf{y}^*} \mathbf{T}$ is the Jacobian

matrix of \mathbf{T} evaluated at \mathbf{y}^* ; and $\check{\mathbf{D}}$ is the diagonal matrix of the standard deviations of $\check{\mathbf{y}}$, defined as $\check{\mathbf{y}} = \mathbf{y}^* + (\mathbf{u} - \mathbf{u}^*) \mathbf{J}_{\mathbf{u}^*, \mathbf{y}^*}^{-1}$. The positive sign of the importance measure implies that the random variable is a load variable, and the negative sign implies that the random variable is a resistance variable. Also, the magnitude of the importance measure represents the random variable's contribution to the limit-state function variance.

4.3. Reliability analysis of an example RC beam under blast loading

In this section, we develop fragility functions for an example RC beam subject to blast loading. Table 4 summarizes the beam's geometry and material properties and, when appropriate, their statistical information. The distance between the beam and the trinitrotoluene (TNT) explosive charge is 10 m; this distance allows us to satisfy the planar blast wave hypothesis. The scaled distance z varies from 0.6 to 2.4 m/kg^{1/3} by changing the quantity of the explosive TNT charge.

In general, the mechanical properties of materials is much more challenging to quantify than geometrical sizes, which can be easily determined with high accuracy and are usually considered as deterministic variables. In addition, geometrical imperfection proved to have a negligible influence on the reliability analysis as shown in [15, 35, 57].

Table 4: Summary of design variables for the example beam

Variable	Value/Mean	CoV	Distribution
l [m]	1.5	-	-
H [m]	0.16	-	-
b [m]	0.3	-	-
μ [kg/m]	120	-	-
f_{cc} [MPa]	40	0.15	Lognormal
f_{sy} [MPa]	450	0.05	Lognormal
E_s [GPa]	210	-	-
$\rho_s = A_s / (bH)$	0.209	-	-
A_s / A_{ss}	0.1563	-	-

Figure 6 shows the computed fragility functions for the three damage levels in Table 3. The solid curves in the figure represent the predictive estimate of the fragility function $\tilde{F}(z)$. The shaded area around the predictive estimate represents the [0.15, 0, 85] confidence band due to the statistical uncertainty in the estimate of Θ . The computed fragility functions can be useful to design an optimal stand-off distance for given design requirements. For example, to design a beam with the characteristics described in Section 2 for a given explosive charge mass (i.e., 50 kg) and the probability of exceeding the limit-state threshold (i.e., 99%), the necessary stand-off distances to reach the three damage levels are blowout 2.56 m, heavy damage

351 4.05 m, and moderate damage 5.16 m. This information can also help to design protective fences around
352 structures that can guarantee a specific stand-off distance.

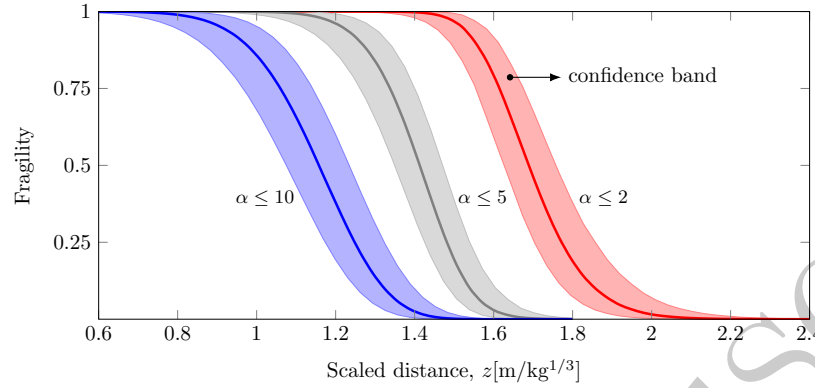


Figure 6: Fragility functions for the three damage levels

353 Figure 7 shows the computed importance measures of random variables f_{sy} , f_{cc} , and ε for the three
354 damage levels. For each damage level, the importance measures are computed for different values of the
355 scaled distance z , ranging from 0.6 to 2.4 $\text{m/kg}^{1/3}$. In this way, it is possible to identify the influence of the
356 selected random variables on the beam's failure probability for different loading levels. The most important
357 variable to the failure event is the model error. This result explains that uncertainty in material properties
358 has negligible effects on the failure probability estimate. Thus, future work may focus on the improvement
359 of the probabilistic model.

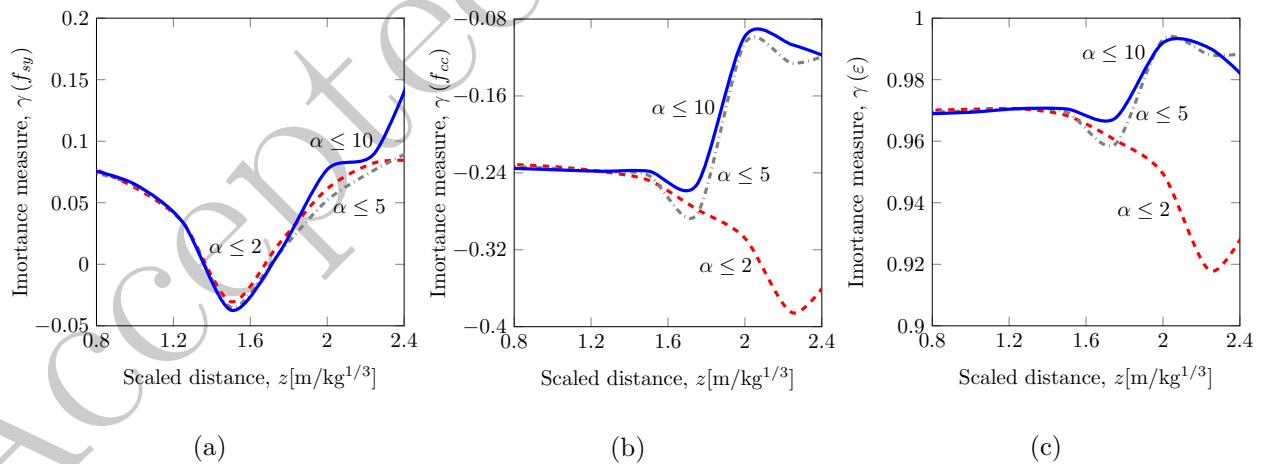


Figure 7: Importance measures of f_{sy} (a), f_{cc} (b), and ε (c) to the failure event

5. Conclusions

The paper proposed a novel probabilistic demand model for reinforced concrete (RC) beams under blast loading that is computationally convenient for reliability analysis while capturing the governing physical laws. The proposed model combines the prediction from a simplified physics with an analytical correction term. Specifically, the dynamics of an RC beam has been captured by an equivalent generalized single-degree-of-freedom (SDOF) system, derived from the conservation law of energy using smooth material constitutive laws and bending moment-curvature relationship. The correction term is then developed to capture the compromises in the simplified physics (i.e., the generalized SDOF representation.) The paper presented Bayesian inference to estimate the unknown model parameters in the correction term and the model error from experimental data and any prior information. Integrating the predictions from the generalized SDOF system into the proposed model enables the best use of limited experimental data to develop a general probabilistic demand model. The conditional failure probability (i.e., fragility function) are then obtained from rigorous reliability analyses using the proposed probabilistic demand model. The fragility function was conditioned on the scaled distance from the explosive discharge as the hazard intensity measure. Implementing the smooth material constitutive laws and bending moment-curvature relationship enabled using the First Order Reliability Method (FORM) to estimate the fragility function, which is several orders of magnitude faster than sampling methods; it also provides the importance measures of random variables with no additional calculations. Fragility functions can help us to design the stand-off distance such that the blast-induced damage does not exceed a given level with the desired confidence. As an illustration, the paper estimated the fragility functions of an example RC beam for three damage levels. The calculated importance measures indicate that the primary source of uncertainty in reliability analyses is the model error. Thus, future work should improve the simplified physics and develop a more informative correction term using additional data.

Acknowledgments

The financial support by Autonomous Region of Sardinia under grant PO-FSE 2014-2020, CCI: 2014-IT05SFOP021, through the project "Retrofitting, rehabilitation and requalification of the historical cultural architectural heritage (R3-PAS)" is acknowledged by Flavio Stochino.

387 **Appendix A. Experimental Database**

388

Accepted Manuscript

Table A.5: Synthesis of the experimental database

Beam	z [m/kg ^{1/3}]	P_r [kPa]	t_d [msec]	I [kPa-sec]	ρ [kN/m ³]	f_{cu} [MPa]	ϵ_{cu} [%]	f_{sy} [MPa]	ρ_s [%]	v_{max} [mm]
1	21.99	650	23	3.76	25.0	43	0.35	604	2.64	9.4
2	11.00	1,044	25	5.40	25.0	43	0.35	604	2.64	16.6
3	12.10	1,060	26	5.57	25.0	43	0.35	604	2.64	14.6
4	16.13	780	22	4.70	25.0	43	0.35	604	2.64	12
5	9.68	1,249	22	6.38	25.0	43	0.35	604	2.64	17.5
6	9.68	1,272	21	6.67	25.0	43	0.35	604	2.64	23.6
7	16.13	998	25	5.33	25.0	109	0.30	604	2.64	18.6
8	9.68	1,459	20	6.44	25.0	109	0.30	604	2.64	25.4
9	6.91	1,675	16	6.74	25.0	109	0.30	604	2.64	24.1
10	24.19	720	36	5.36	25.1	81	0.28	580	1.21	17
11	12.10	1,059	26	5.91	25.0	81	0.28	580	1.21	22.9
12	8.10	1,946	30	9.58	25.2	81	0.28	580	1.21	44.6
13	24.19	680	34	4.54	28.5	133	0.30	580	1.78	8.7
14	12.10	1,186	25	6.83	28.8	133	0.30	580	1.77	13.8
15	8.06	1,907	28	9.50	28.8	133	0.30	580	1.77	26.6
16	6.05	1,906	29	11.54	28.9	173	0.30	555	2.70	29.3
17	8.06	1,876	31	9.27	29.2	173	0.30	555	2.68	17.7
18	6.91	1,957	30	10.21	29.4	173	0.30	555	2.75	17.8
19	12.10	1,341	28	7.42	24.3	92	0.30	544	1.81	37
20	9.68	1,558	27	8.34	24.3	92	0.30	544	1.81	38.9
21	8.06	1,859	30	9.40	24.3	92	0.30	544	1.81	46.4

389 **References**

- 390 [1] C. Pearson, N. Delatte, Ronan point apartment tower collapse and its effect on building codes, *Journal*
391 *of Performance of Constructed Facilities* 19 (2005) 172–177.
- 392 [2] P. Kotsovinos, A. Usmani, The world trade center 9/11 disaster and progressive collapse of tall buildings,
393 *Fire Technology* 49 (2013) 741–765.
- 394 [3] B. Keane, P. Esper, Forensic investigation of blast damage to British buildings, in: *Proceedings of the*
395 *Institution of Civil Engineers-Civil Engineering*, 5, 2009, pp. 4–11.
- 396 [4] S. Rigby, T. Lodge, S. Alotaibi, A. Barr, S. Clarke, G. Langdon, A. Tyas, Preliminary yield estimation
397 of the 2020 Beirut explosion using video footage from social media, *Shock Waves* 30 (2020) 671–675.
- 398 [5] D. Zhang, S. Yao, F. Lu, X. Chen, G. Lin, W. Wang, Y. Lin, Experimental study on scaling of RC
399 beams under close-in blast loading, *Engineering Failure Analysis* 33 (2013) 497–504.
- 400 [6] S.-j. Yao, D. Zhang, F.-y. Lu, W. Wang, X.-g. Chen, Damage features and dynamic response of RC
401 beams under blast, *Engineering Failure Analysis* 62 (2016) 103–111.
- 402 [7] J. Magnusson, M. Hallgren, High performance concrete beams subjected to shock waves from air blast,
403 *Technical Report FOA-R-00-01586-311-SE*, Swedish Defence Research Agency (FOA), Tumba, Sweden,
404 2002.
- 405 [8] J. Magnusson, M. Hallgren, High performance concrete beams subjected to shock waves from air blast,
406 *Part 2, Technical Report FOI-R-1116-SE*, Swedish Defence Research Agency (FOI), Tumba, Sweden,
407 2003.
- 408 [9] J. Magnusson, M. Hallgren, A. Ansell, Air-blast-loaded, high-strength concrete beams. Part I: Experi-
409 mental investigation, *Magazine of Concrete Research* 62 (2010) 127–136.
- 410 [10] Z. Liao, D. Tang, Z. Li, Y. Xue, L. Shao, Study on explosion resistance performance experiment
411 and damage assessment model of high-strength reinforcement concrete beams, *International Journal of*
412 *Impact Engineering* 133 (2019) 103362.
- 413 [11] C. Zhai, L. Chen, H. Xiang, Q. Fang, Experimental and numerical investigation into RC beams subjected
414 to blast after exposure to fire, *International Journal of Impact Engineering* 97 (2016) 29–45.
- 415 [12] J.-Y. Lee, H. Aoude, Y.-S. Yoon, D. Mitchell, Impact and blast behavior of seismically-detailed RC and
416 UHPFRC-strengthened columns, *International Journal of Impact Engineering* (2020) 103628.

- 417 [13] A. Jahami, Y. Temsah, J. Khatib, The efficiency of using CFRP as a strengthening technique for
418 reinforced concrete beams subjected to blast loading, *International Journal of Advanced Structural*
419 *Engineering* 11 (2019) 411–420.
- 420 [14] F. Stochino, G. Carta, SDOF models for reinforced concrete beams under impulsive loads accounting
421 for strain rate effects, *Nuclear Engineering and Design* 276 (2014) 74–86.
- 422 [15] F. Stochino, RC beams under blast load: Reliability and sensitivity analysis, *Engineering Failure*
423 *Analysis* 66 (2016) 544–565.
- 424 [16] K. Singh, P. Gardoni, F. Stochino, Probabilistic models for blast parameters and fragility estimates of
425 steel columns subject to blast loads, *Engineering Structures* 222 (2020) 110944.
- 426 [17] W. Riedel, K. Fischer, C. Kranzer, J. Erskine, R. Cleave, D. Hadden, M. Romani, Modeling and
427 validation of a wall-window retrofit system under blast loading, *Engineering Structures* 37 (2012) 235–
428 245.
- 429 [18] J. Li, H. Hao, A two-step numerical method for efficient analysis of structural response to blast load,
430 *International Journal of Protective Structures* 2 (2011) 103–126.
- 431 [19] A. Hussein, H. Mahmoud, P. Heyliger, Probabilistic analysis of a simple composite blast protection wall
432 system, *Engineering Structures* 203 (2020) 109836.
- 433 [20] F. Stochino, A. Attoli, G. Concu, Fragility curves for RC structure under blast load considering the
434 influence of seismic demand, *Applied Sciences* 10 (2020) 445.
- 435 [21] United States Department of Defense, Structures to resist the effects of accidental explosions, Technical
436 Report UFC 3-340-02, Unified Facilities Criteria, Washington, DC, 2008.
- 437 [22] G. Carta, F. Stochino, Theoretical models to predict the flexural failure of reinforced concrete beams
438 under blast loads, *Engineering Structures* 49 (2013) 306–315.
- 439 [23] B. Yan, F. Liu, D. Song, Z. Jiang, Numerical study on damage mechanism of RC beams under close-in
440 blast loading, *Engineering Failure Analysis* 51 (2015) 9–19.
- 441 [24] X. Ye, C. Zhao, K. He, L. Zhou, X. Li, J. Wang, Blast behaviors of precast concrete sandwich EPS
442 panels: FEM and theoretical analysis, *Engineering Structures* 226 (2021) 111345.
- 443 [25] M. D. Netherton, M. G. Stewart, The effects of explosive blast load variability on safety hazard and
444 damage risks for monolithic window glazing, *International Journal of Impact Engineering* 36 (2009)
445 1346–1354.

- 446 [26] W. Zhao, J. Qian, Resistance mechanism and reliability analysis of reinforced concrete columns subjected
447 to lateral impact, *International Journal of Impact Engineering* 136 (2020) 103413.
- 448 [27] K.-C. Wu, B. Li, K.-C. Tsai, The effects of explosive mass ratio on residual compressive capacity of
449 contact blast damaged composite columns, *Journal of Constructional Steel Research* 67 (2011) 602–612.
- 450 [28] H. Hao, Y. Hao, J. Li, W. Chen, Review of the current practices in blast-resistant analysis and design
451 of concrete structures, *Advances in Structural Engineering* 19 (2016) 1193–1223.
- 452 [29] H. Sharma, P. Gardoni, S. Hurlebaus, Probabilistic demand model and performance-based fragility
453 estimates for rc column subject to vehicle collision, *Engineering Structures* 74 (2014) 86–95.
- 454 [30] Y. Sha, H. Hao, Laboratory tests and numerical simulations of barge impact on circular reinforced
455 concrete piers, *Engineering Structures* 46 (2013) 593–605.
- 456 [31] C. Demartino, J. Wu, Y. Xiao, Response of shear-deficient reinforced circular rc columns under lateral
457 impact loading, *International Journal of Impact Engineering* 109 (2017) 196–213.
- 458 [32] A. Nghiem, C. Demartino, Y. Xiao, T. H. Kang, Impact behavior of unbonded post-tensioned concrete
459 beams, *ACI Structural Journal* 118 (2021) 201–214.
- 460 [33] O. Ditlevsen, H. O. Madsen, *Structural reliability methods*, Wiley, New York, NY, 1996.
- 461 [34] P. Gardoni, *Risk and reliability analysis: Theory and applications*, Springer International Publishing,
462 2017.
- 463 [35] P. Gardoni, A. Der Kiureghian, K. Mosalam, Probabilistic capacity models and fragility estimates for
464 reinforced concrete columns based on experimental observations, *Journal of Engineering Mechanics* 128
465 (2002) 1024–1038.
- 466 [36] A. Tabandeh, P. Gardoni, Probabilistic capacity models and fragility estimates for RC columns
467 retrofitted with FRP composites, *Engineering Structures* 74 (2014) 13–22.
- 468 [37] A. Tabandeh, P. Asem, P. Gardoni, Physics-based probabilistic models: Integrating differential equa-
469 tions and observational data, *Structural Safety* 87 (2020) 101981.
- 470 [38] G. E. Box, G. C. Tiao, *Bayesian inference in statistical analysis*, John Wiley & Sons, New York, NY,
471 2011.
- 472 [39] C. R. Rao, H. Toutenburg, *Linear models: least squares and alternatives*, Springer-Verlag, New York,
473 NY, 1995.

- 474 [40] G. E. Box, D. R. Cox, An analysis of transformations, *Journal of the Royal Statistical Society: Series*
475 *B (Methodological)* 26 (1964) 211–243.
- 476 [41] M. Laine, Adaptive MCMC methods with applications in environmental and geophysical models, Ph.D.
477 thesis, Lappeenranta University of Technology, Lappeenranta, Finland, 2008.
- 478 [42] A. Gelman, J. B. Carlin, H. S. Stern, D. B. Rubin, *Bayesian data analysis*, Chapman & Hall/CRC,
479 Boca Raton, FL, 2013.
- 480 [43] F. Freidlander, The diffraction of sound pulses I. Diffraction by a semi-infinite plate, *Proceedings of*
481 *the Royal Society A* 186 (1946) 322–344.
- 482 [44] P. Olati, F. Petrini, K. Gkoumas, Fragility analysis for the performance-based design of cladding wall
483 panels subjected to blast load, *Engineering Structures* 78 (2014) 112–120.
- 484 [45] C. Mills, The design of concrete structures to resist explosions and weapon effects, in: *Proceedings of*
485 *the 1st International Conference for Hazard Protection*, Edinburgh, Scotland, 1987, pp. 27–30.
- 486 [46] M. Held, Blast waves in free air, *Propellants, Explosives, Pyrotechnics* 8 (1983) 1–7.
- 487 [47] Comité Euro-international du Béton (CEB), *Concrete structures under impact and impulsive loading*,
488 *Technical Report, Bulletin d'information*, Lausanne, Switzerland, 1988.
- 489 [48] *Model Code, First complete draft, Volume 1, Technical Report*, Comité Euro-International du Béton
490 *Secretariat Permanent*, CH-1015 Lausanne, Switzerland, 2010.
- 491 [49] P. Cox, P. Westine, J. Kulesz, E. Esparza, *Analysis and evaluation of suppressive shields*, *Technical*
492 *Report*, Southwest Research Institute, San Antonio, Texas, 1978.
- 493 [50] T. P. Ryan, *Modern engineering statistics*, Wiley-Interscience, Hoboken, NJ, 2007.
- 494 [51] P. Gardoni, R. G. Pillai, M. B. D. Hueste, K. Reinschmidt, D. Trejo, Probabilistic capacity models for
495 corroding posttensioning strands calibrated using laboratory results, *Journal of Engineering Mechanics*
496 135 (2009) 906–916.
- 497 [52] A. Der Kiureghian, Measures of structural safety under imperfect states of knowledge, *Journal of*
498 *Structural Engineering* 115 (1989) 1119–1140.
- 499 [53] C. Murphy, P. Gardoni, C. E. Harris, Classification and moral evaluation of uncertainties in engineering
500 modeling, *Science and Engineering Ethics* 17 (2011) 553–570.

- 501 [54] United States Army Corps of Engineers (USACE), Single degree of freedom structural response limits
502 for antiterrorism design, Technical Report PDC-TR 06-08, Protective Design Center (PDC), Omaha,
503 NE, 2008.
- 504 [55] P. Gardoni, K. M. Mosalam, A. Der Kiureghian, Probabilistic seismic demand models and fragility
505 estimates for RC bridges, *Journal of Earthquake Engineering* 7 (2003) 79–106.
- 506 [56] A. Der Kiureghian, First-and second-order reliability methods, in: E. Nikolaidis, D. M. Ghiocel,
507 S. Singhal (Eds.), *Engineering Design Reliability Handbook*, CRC Press, Boca Raton, FL, 2004, pp.
508 465–494.
- 509 [57] D.-E. Sha, P. Gardoni, D. Rosowsky, Closed-form fragility estimates, parameter sensitivity, and bayesian
510 updating for rc columns, *Journal of Engineering Mechanics* 137 (2007) 833–843.